Korean J. Chem. Eng., 36(11), 1900-1914 (2019)
DOI: 10.1007/s11814-019-0376-x

pISSN: 0256-1115
eISSN: 1975-7220

Hazardous As(III) removal using nanoporous activated carbon of waste garlic stem as adsorbent: Kinetic and mass transfer mechanisms

Anuj Kumar Prajapati and Monoj Kumar Mondal†

Department of Chemical Engineering and Technology, Indian Institute of Technology (Banaras Hindu University), Varanasi, Uttar Pradesh 221005, India
(*Received 9 April 2019 • accepted 28 August 2019*)

Abstract–Nanoporous activated garlic stem carbon (AGSC) was prepared from garlic stem waste and used to remove As(III)from synthetic water under complete batch experiments. Characterization studies of AGSC were performed by FTIR, SEM, EDX, BET, XPS and XRD techniques. Batch adsorption experiments were carried out to study the adsorption of As(III) onto AGSC. Maximum removal of 93.3% of As(III) was obtained at optimum condition of pH 6, the adsorbent dose 5 g/L, equilibrium time 150 min, initial As(III) concentration 400 μg/L and temperature 298 K. Both Langmuir and Temkin isotherm model fitted well to the experimental data as compared to Freundlich isotherm. Kinetics indicated that the adsorption of As(III) was more suitable for pseudo-second-order than pseudo-first-order and Elovich model. The mass transfer mechanism could be described by Weber-Morris and Boyd mass transfer model. The maximum adsorption capacity of AGSC for As(III) removal was found to be 192.30 μg/g. The negative enthalpy and free energy change indicated that the adsorption process of As(III) onto AGSC was exothermic and spontaneous. The negative value of entropy change suggested decreasing randomness at the AGSC-aqueous As(III) interface during As(III) adsorption.

Keywords: As(III) Adsorption, AGSC Characterization, Kinetics, Mass Transfer Models and Desorption

INTRODUCTION

Every form of life on the earth is dependent on water directly or indirectly. The earth surface is comprised of about 71 percent water. Still, there is a scarcity of water because only 1 percent out of the total water is available for mankind. This one percent of fresh water has many problems, like the presence of heavy metals and other toxic pollutants, which make it unsafe for use. Over 60% of the total world population use groundwater for drinking and household activities. Most of the countries, and India as well, where nearly 80% rural and almost 51% urban water supply is provided by groundwater source alone [1]. Arsenic is one of the most toxic metalloids present in groundwater and other water bodies. It has hazardous effects on humans, animals and plants. Countries like China, India, Nepal, Bangladesh, Taiwan, Japan, Mexico, United States, and Canada are facing the problem of arsenic contamination [2,3]. In India and Bangladesh, more than 100 million people are using drinking water containing arsenic concentration of more than 1 mg/L. According to the WHO report, more than 2.5 billion people do not have proper and safe water accessibility. It is also estimated that 2.0 billion people are using contaminated drinking water [4]. Arsenic is carcinogenic and ranks 20^{th} in plenty in the earth layer, 14^{th} in ocean water that holds about more than 96% of all earth's pool, and 12^{th} in the human body [5]. Natural and anthropogenic are two types of sources of arsenic contamination, but anthropogenic sources are primarily responsible for arsenic contamination than natural sources, and these include industries like gold mining, non-ferrous smelting, petroleum-refining, and mining activities [6]. Its minimal concentration can also cause skin thickening (hyperkeratosis), hepatocellular carcinoma, hypertension, neurological disorders, melanosis, muscular weakness, cirrhosis, liver fibrosis, loss of appetite, nausea and parenchymal cell damage [7]. The regular consumption of arsenic contaminated water can be fatal and causes different types of cancer like skin, lungs, bladder, and kidneys. The inorganic form of arsenic is found in the form of oxides (As_2O_3, As_2O_5), which are highly toxic [8]. Arsenic is found in various oxidation states (e.g., −3, 0, +3, and +5), but it is mostly found in trivalent (As(III)) and pentavalent (As(V)) form. Arsenate (As(V)) form predominates in oxygen-rich aerobic condition [9]. Arsenite (As(III)) predominates in the absence of free oxygen condition, such as groundwater and shows ten-times more toxicity than arsenate [10]. The toxicity of arsenic species follows the increasing order as elemental forms of arsenic<compounds of arsonium<pentavalent organic compounds< forms of inorganic arsenates<trivalent organic compounds (arsenoxides)<inorganic arsenates<arsines [11].

Due to the lethal effects of arsenic, the environmental protection agencies of various countries have set several rules to determine the acceptable concentration of arsenic in water. In 2001, US EPA and WHO updated the maximum toxicity level for total arsenic in consumption water for human use from 50 to 10 μg/L. To keep the concentration of arsenic below 10 μg/L, several technologies have been used, including ion-exchange [12], electrochemical [13], coagulation-flocculation [14,15], membrane [16] and adsorption [17]. Except for adsorption, all these technologies are often high process cost, low removal efficiency, use of toxic reagents and fail to concentrate arsenic in small waste volumes [8]. Adsorption process can be made

†To whom correspondence should be addressed.
E-mail: mkmondal13@yahoo.com

economical if the adsorbent is prepared from abundantly available waste materials, inexpensive preparation technologies, and good regeneration ability. The adsorption phenomenon mainly depends on adsorbent capacity, selectivity and reversibility [18].

In the present study, waste garlic stem was used to synthesize nanoporous activated garlic stem carbon (AGSC). AGSC has been used as an adsorbent to remove arsenic (III) from synthetic water as well as groundwater. In garlic production, India is the second largest country in the world, due to which it produces a large amount of waste garlic stem. Garlic stem is a waste burnt by the farmers that decreases the air quality. For this reason, the authors chose the waste garlic stem for production of active carbon. Batch adsorption experiments were performed to examine the effect of equilibrium time, initial pH, AGSC dose, initial As(III) concentration and temperature on adsorption of As(III). The BET, SEM, EDX, FTIR, XRD and XPS analysis were also performed on the AGSC before and after adsorption experiments. The adsorption isotherm and kinetic models were also investigated and fitted with experimental data. The critical reaction mechanism of As(III) adsorption onto AGSC was also discussed. The mass transfer mechanism and thermodynamics of adsorption process were also studied, and all the parameter values were determined. The effect of co-existing anions like sulfate, phosphate, chloride and nitrate on adsorption efficiency was also reported. The regeneration process of AGSC adsorbent was also examined.

MATERIALS AND METHODS

1. Equipment and Chemicals

All analytical grade reagents were purchased from S. D. Fine-Chem Ltd and Merck Chemical, India and used without purification for experimental work. Deoxygenated water and double distilled was used during experimentation as and when required. The waste garlic stem was dried with a hot air oven (S.M.S.I. Pvt. Ltd., India). NSW-104 split tubular furnace single zone (Narang Scientific Works Pvt. Ltd, India), N_2 and CO_2 gas (99.9% purity) were used for the preparation of activated carbon from waste garlic stem. The stock solution of As(III) of 1,000 μg/L concentration was prepared by dissolving an appropriate quantity of sodium arsenite ($NaAsO_2$) in deoxygenated water. A pH meter (LI 120, Elico India) was used for measuring the pH of the As(III) sample. For batch adsorption, the pH of the As(III) solution was adjusted using 0.1 M HNO_3/KOH solution. A shaking speed incubator (model NSW-133, Calton New Delhi, India) was used for proper mixing between adsorbent and adsorbate solution. After adsorption, the concentration of As(III) in the filtrate was analyzed by using an inductively coupled plasma (ICP) spectrometer (ICAP 6300, Thermo Fisher Scientific, USA).

2. Preparation of Adsorbent

Waste garlic stem was collected from hostel canteen of Indian Institute of Technology (BHU), Varanasi. First, it was washed with tap water followed by double distilled water two times to remove surface impurities. Then, it was kept in an oven for 24 hours at 80 °C. The dried garlic stem was converted into fine particles by a mixer grinder, and the particles passed through 85 mesh but retained on 150 mesh (0.105-0.170 mm size) were taken for the production of activated garlic stem carbon. The process for preparing activated garlic stem carbon was carried out in the stainless-steel reactor (520 mm length, 44 mm inner and 48 mm outer diameter) placed in a split tube furnace. For carbonization process, 20 g of sieved garlic stem particles was taken on metal mesh in the reactor and then heated from room temperature to 500 °C at a constant heating rate of 10 °C/min with N_2 (99.98% purity) gas flow of 150 cm^3/min. Thereafter, the sample was held at 500 °C for 1 hour in N_2 gas flow condition. After the carbonization process, the sample was activated by CO_2 gas for a further one hour with a constant flow rate of 200 cm^3/min at 700 °C. Finally, the reactor was cooled under inert gas flow of N_2. Thus, prepared activated carbon was further ground into fine particles, and the fine ground particles were sieved through 150 to 200 mesh size sieves. The particle size between 75-105 μm was stored in airtight glass container experimental work. This obtained fine powder was termed as activated garlic stem carbon (AGSC).

3. Characterization of AGSC

The net electrical charge density on the surface of AGSC adsorbent was examined with the point of zero charge (pH_{pzc}) by solid addition method [19]. The specific surface area and other surface properties of AGSC were characterized with an ASAP 2020 adsorption apparatus (Micromeritics, USA), using N_2 gas as the adsorbate at 77 K. The specific surface area (SSA_{BET}) was determined by the Brunauer-Emmett-Teller (BET) equation. The t-plot method was used to obtain micropore surface area (S_{micro}), external surface area (S_{ext}) and micropore volume (V_{micro}). The single point total pore volume (V_T) was obtained from the adsorption isotherm at P/P_0= 0.989. The mesopore area (S_{meso}) and mesopore volume (V_{meso}) were obtained by the deduction of S_{micro} from SSA_{BET} and V_{micro} from V_T, respectively. BJH adsorption dV/dD pore volume method was used for PSD analysis. Powder X-ray diffraction (XRD) analysis of AGSC was carried out by using Phillips 1710 X-ray diffractometer with the help of cu-kα monochromatic radiation in the Bragg's angle (2θ) range of 5-90°. Investigation of functional groups present onto AGSC (before and after As (III) adsorption) was done by Fourier transform infrared spectroscopy (Nicolet 5700 FTIR, Thermo Electron Corp., USA) analysis with the wave number range 4,000-400 cm^{-1} by using KBr pellets (AGSC : KBr:: 1: 100). The scanning electron microscope (SEM) equipped with energy dispersive X-ray spectroscopy (EDX) was used for investigation of the surface morphologies and chemical composition of AGSC and As(III) loaded AGSC adsorbent using ZEISS, EVO 18, Germany. The type of chemical element and their bond formation between them were examined through X-ray photoelectron spectroscopy (XPS) (AMICUS, Kratos Analytical, Shimadzu Group Company) analysis with the help of Mg-K_α (1,253.6 eV) a monochromatic X-ray radiation source.

4. Batch Adsorption Experiments

The batch mode operation of the adsorption experiment was used to study the removal of As(III) from the liquid phase by using AGSC as an adsorbent. The adsorption experiments were carried out by adding the desired amount of AGSC in 50 ml of the As(III) solution of predetermined concentration in the 100 mL conical flasks at a fixed pH value. Then the conical flasks containing solution were agitated in shaking speed incubator at 25 °C and 150 rpm for a time until reaching an equilibrium condition. The conical flask was removed from the incubator at the end of the predetermined time

interval, and liquid samples were filtered and the supernatant liquid was analyzed by ICP spectrometer to find the residual concentration of As(III) ions. Table S1 presents the entire experimental condition for batch adsorption of As(III) on AGSC. The adsorption capacity of AGSC and percentage removal As(III) ions were calculated according to Eq. (1) and Eq. (2), respectively.

$$q_e = \frac{C_i - C_e}{M} \times V \quad (1)$$

$$\%R = \frac{C_i - C_e}{C_i} \times 100 \quad (2)$$

where q_e the adsorbed As(III) ions per unit mass of AGSC in g/g, C_i and C_e are the initial concentration of As(III) ions and concentration of As(III) ions at equilibrium in (g/L), respectively. V and M are the volume of solution in liter (L) and M is the amount of AGSC adsorbent used in gram (g), respectively. The effect of co-existing anions such as sulfate, phosphate, chloride and nitrate, which are commonly present in ground water, was also studied with concentration ranging from 0 to 1,000 μg/L. The concentration of sodium, calcium and potassium in the groundwater and AGSC treated groundwater was determined with an ESICO-1382 microprocessor flame photometer. The concentration of Iron, SO_4^-, Cl^-, and NO_3^- was analyzed by colorimetric, nephelometric, iodometric titration, and spectrophotometric method, respectively. Desorption study of As(III) from the exhausted AGSC was investigated with 0.05 M to 2.5 M solution of NaOH.

RESULTS AND DISCUSSION

1. Characterization of the AGSC Adsorbents

1-1. BET and XRD Analysis

The occurrence of the hysteresis loop in N_2 adsorption isotherms at low temperature is usually related to capillary condensation in mesopore structures of the sample. Generally, the reason for formation of different hysteresis loops is based on the different type of adsorbents characteristic and condition for adsorption (pressure and temperature). Fig. 1(a) and 1(b) shows the N_2 adsorption-desorption isotherm and pore size distribution (PSD) plots of AGSC adsorbent, respectively. From Fig. 1(a), the adsorbent AGSC has a sharp increase in nitrogen adsorption capacity (68 to 75 cm^3/g STP) at low relative pressure range (p/p^o<0.2) because of

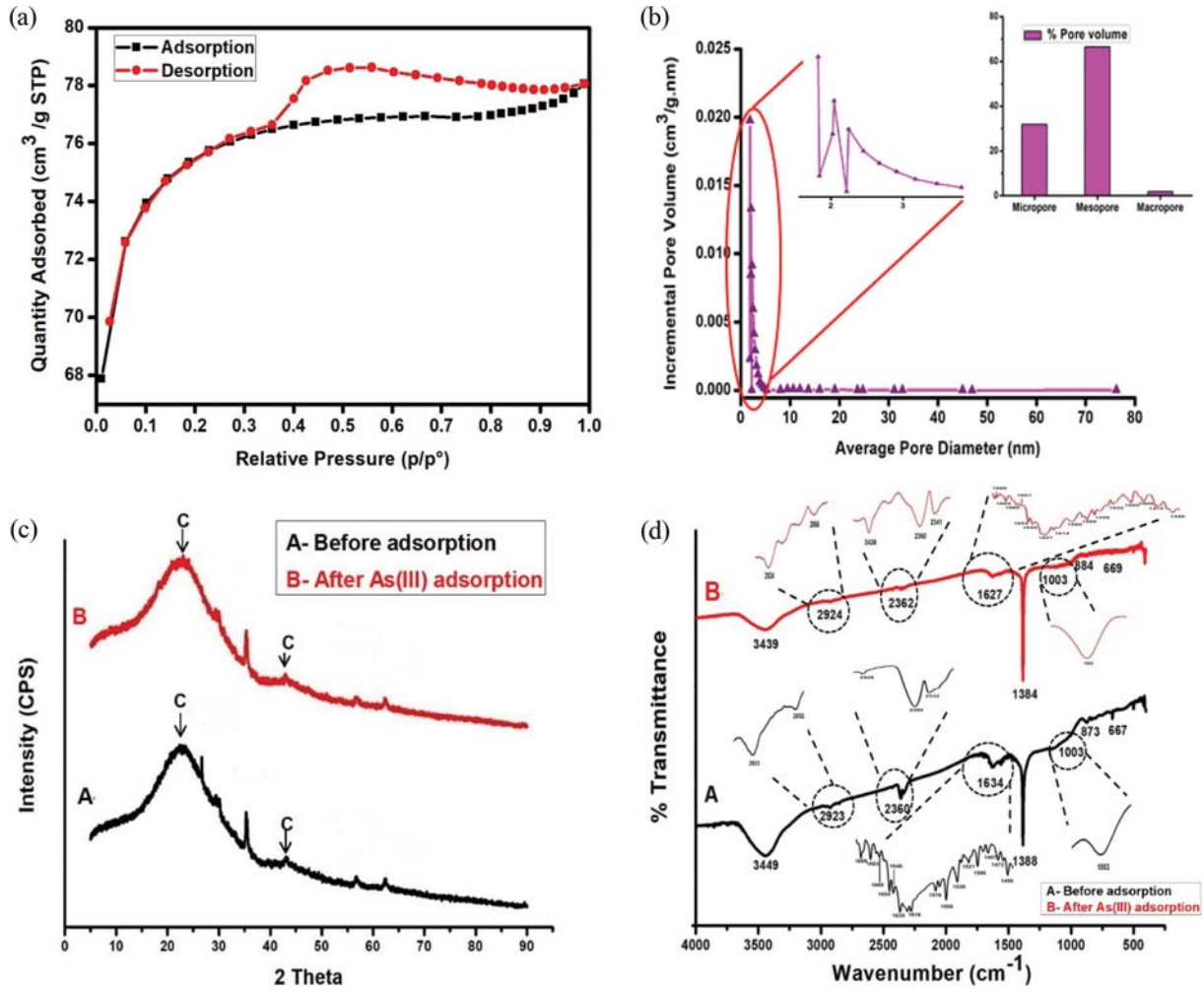

Fig. 1. (a) N_2 adsorption-desorption isotherm, (b) pore size distribution (PSD), (c) X-ray diffraction (XRD) pattern and (d) FTIR spectra of AGSC.

micropore filling effect. Nitrogen adsorption capacity constant at medium relative pressure range ($0.4<p/p^o>0.8$) behaves like multilayer sorption, and very little increase in nitrogen adsorption capacity at high relative pressure range ($p/p^o>0.8$) because of capillary condensation; this behavior of curve indicated that the adsorption/desorption isotherm of AGSC adsorbent is type I-B. The hysteresis loop is present in relative pressure range of 0.4-1.0, which belongs to type H2(a) loop [20]. These results suggest that the surface structure of AGSC adsorbent has the existence of both microporous and mesoporous pores. This was also confirmed by SEM image. PSD curve can be used for qualitative analysis purpose, which gives the information about prevailing pore size, the major peak of PSD and pore size range. Form the Fig. 1(b) it can be concluded that the majority of pores' size appeared in the mesopore region (2 nm to 20 nm) and minor occurs in micropore size region (below 2 nm). For the AGSC sample, the dominant mesopore size is between 2 and 6 nm, with two major peaks at approximately 2.064 nm and 2.25 nm (shown in zoom part of Fig. 1(b)). One high-intensity peak is also shown in the micropore size region, which is at approximately 1.82 nm. It is also confirmed by the pore volume percentage graph (Fig. 1(b)). In AGSC adsorbent, approximately 66.42% pores occur in the mesopores and 31.81% in micropore region [21].

All textural properties related to the surface are summarized in Table S2. The BET surface area, average pore diameter (D_p) and micropore volume (V_{micro}) of the AGSC adsorbent were 227.62 m^2/g, 2.09 nm and 0.10 cm^3/g, respectively. It was much higher than other chemically prepared activated carbons [22] as well as raw garlic peel waste as reported by Hameed and Ahmad [23].

The structural property of AGSC sample was determined by X-ray diffraction pattern. Fig. 1(c) shows the XRD plots of the AGSC before and after As(III) loading. XRD spectrum of the AGSC sample shows a broad diffraction peak at approximately $2\theta=23^o$ and a weak peak at approximately $2\theta=44^o$ which is related to the (002) and (100) planes of graphitic carbon. The broad and low intensity of the peaks indicated that the AGSC adsorbent is mostly amorphous nature. Also, in the AGSC adsorbent, which exhibits a few sharp peaks at approximately $2\theta=35^o$, 56^o and 63^o, the presence of those sharp peaks may be attributed to the possibility of residual ash in the carbon [24]. After adsorption, in the As(III) loaded AGSC sample, the intensity of the peak decreased and some peaks disappeared. From this result it was confirmed that the As(III) was absorbed onto the AGSC.

1-2. FTIR Analysis

Fig. 1(d) shows the recorded FTIR spectrum of AGSC before

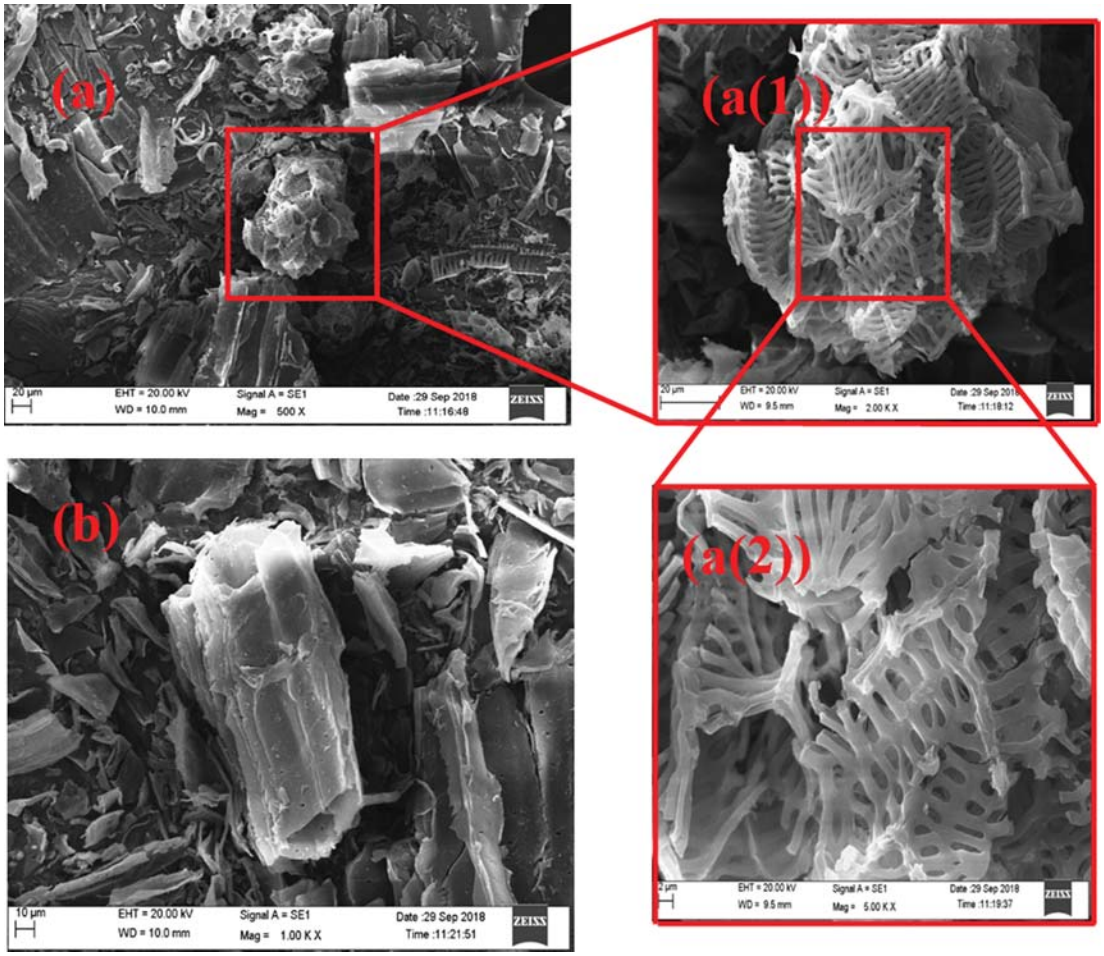

Fig. 2. SEM images of AGSC (a) 500X magnification, (a(1)) 2000X magnification of image a, (a(2)) 5000X magnification of image (a(1)), (b) 1000X magnification at different location of sample.

and after the adsorption of As(III) ions. The FTIR data showed the existence of different types of functional groups on the surface of AGSC. These functional groups are -OH at 3,439 cm^{-1} due to presence of alcohols and phenols, two small intensity peaks of C-H stretching at 2,923 cm^{-1} and 2,852 cm^{-1} due to the presence of aliphatic and the aldehyde or carbohydrate carbon, respectively [25]. The C≡C stretching vibration shows at peak range 2,250-2,450 cm^{-1} due to the existence of alkyne groups [26]. Various low-intensity peaks are shown on the figure in the range of 1,450 to 1,700 cm^{-1}, which suggests C-C and C=C stretching vibration due to aromatic rings and alkenes, respectively, N-H out of plane due to amide and C-O and C=O stretching due to carboxylic, ester, quinone, cyclic b-ketones, aldehyde groups and keto-esters, keto-enol like conjugated groups are present in the AGSC adsorbent [27]. Strong peak intensity observed around 1,388 cm^{-1} could be attributed to the -CH_3 stretching due to alkane compounds [28]. Minimal peak intensity detected at 1,003 cm^{-1} is assigned to the C-O stretching vibration of carboxylic acid and alcohol groups. Two small intensity peaks are present in region of 900-650 cm^{-1} which may be assigned as C-H out of the plane and bending vibration in aromatic rings and alkynes group, respectively [29]. After As(III) adsorption onto AGSC, the two main changes are shown in FTIR spectra. The first one is that the peak intensity and position of -OH stretching vibration was reduced and shifted, respectively [25]. The second is that all peaks were slightly shifted regarding unloaded AGSC adsorbent. The peaks were shifted as given in Table S3.

1-3. SEM-EDX Analysis

The structural morphology of AGSC is shown in Fig. 2(a) and 2(b), which was done by SEM analysis at different magnification and location of the sample. Fig. (2a(1)) and (2a(2)) are the higher

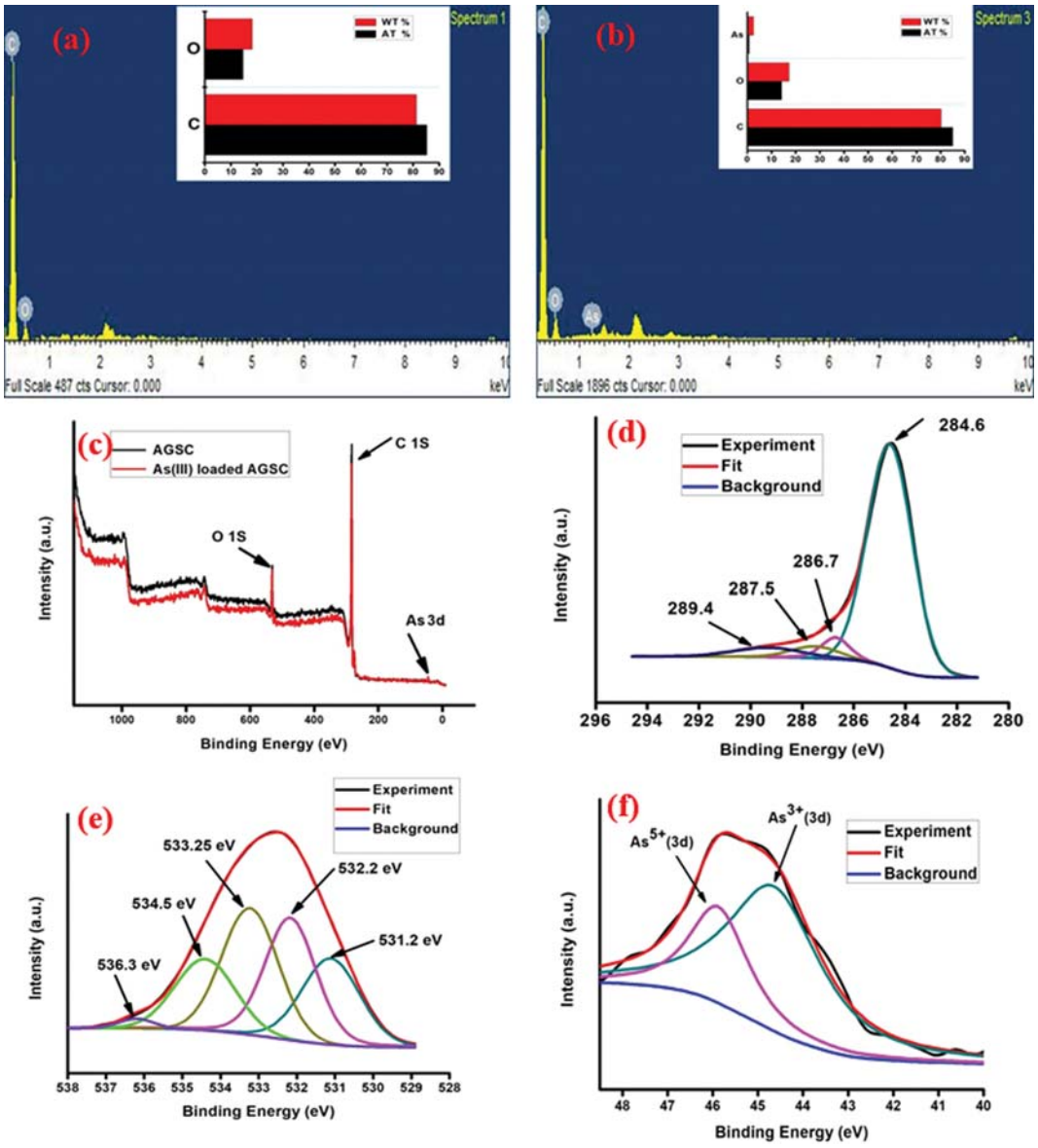

Fig. 3. EDX analysis of (a) AGSC, (b) Arsenic loaded AGSC, (c) XPS wide spectra of AGSC, fitted XPS spectra of (d) C1s, (e) O1s of AGSC before adsorption and (f) As3d spectra of AGSC after arsenic adsorption.

magnification images of Fig. 2(a). After observing the SEM image of AGSC, we concluded that the surface of AGSC was rough, heterogeneous, and contained a considerable number of pores. EDX results of AGSC and As(III) loaded AGSC adsorbent are shown in Fig. 3(a) and 3(b), respectively. The results of the EDX analysis confirmed that carbon and oxygen peak were found in the surface of the AGSC before, and after As(III) adsorption, a small peak of arsenic was also seen in the EDX result. This result confirmed that As(III) was absorbed by AGSC.

1-4. XPS Analysis

XPS is the ultimate characterization technique for investigating the surface composition and oxidation state of an element. Fig. 3(c) shows the wide scan XPS spectra from −10 eV to 1,150 eV of virgin AGSC and As(III) loaded AGSC. From the wide scan XPS diagram of AGSC, the main elements in the structure of AGSC are carbon and oxygen appearing at about approximately 284.3 and 532.9 eV, respectively. The C1s peak appears larger than that of O1s, which means carbon and oxygen are the main components in AGSC and they form different types of bonds which are responsible for As(III) adsorption. There is a small arsenic peak at approximately 44.3 eV along with carbon and oxygen peaks in wide scan XPS diagram of As(III) loaded AGSC, which affirms that As(III) was adsorbed on the surface of AGSC adsorbent.

For the better understanding of chemical properties on the surface of AGSC adsorbent and after As(III) adsorption, XPS Peak 4.1 was applied to deconvolve the high resolution of C1s, O1s and As3d peaks, as shown in Fig. 3(d), 3(e), and 3(f), respectively. Deconvolution of the high resolution C1s spectra consists of four different component peaks. These peaks at approximately 284.6, 286.7 and 289.3 eV can be assigned to C=C (sp^2 hybridized) graphitic carbon, carbon present in alcohol or ether groups and carbon in carboxyl or ester groups, respectively. The weak intense peak at approximately 287.5 eV indicates the presence of carbon in carbonyl or quinone groups [30]. Similarly, Fig. 3(e) shows the high-resolution spectrum of O1s which consisted of five major peaks. These peaks represent different groups such as carbonyl oxygen of quinones at 531.1 eV; carbonyl oxygen in anhydrides, oxygen hydroxyl groups and esters at 532.2 eV; non-carbonyl oxygen atom in anhydrides and esters at 533.2 eV and the oxygen atom in carboxyl groups at 534.3 eV. Fifth and last less intense peak is at approximately 536.1 eV, which can be assigned to adsorbed water and/or oxygen [31]. The result of FTIR also confirmed the existence of these groups.

After adsorption of arsenic in the AGSC adsorbent, a low-intensity peak of arsenic is present in the XPS analysis (Fig. 3(f)). The high resolution spectrum of As3d shows two significant peaks at approximately 44.6 and 45.8 eV, which confirmed that adsorption occurs onto AGSC in the form of As(III) and As(V). The reason for the occurrence of As(V) is the partial change in the oxidation state of As(III). These active functional groups like hydroxyl, carboxylic acid, and ester may be responsible for the adsorption of arsenic species on the surface of the AGSC adsorbent. The results of the C1, O1s and As3d peaks are summarized in Table S4.

2. Arsenic (III) Adsorption Performance

2-1. Effect of Equilibrium Time

Equilibrium time is the time span for which adsorbent and adsorbates come into contact with each other and transfer of the mass from liquid to solid phase until the process does not reach an equilibrium condition [32]. The relationship between removal percentage of As(III) ions and equilibrium time by AGSC is shown in Fig. 5(a). It is clear from the figure that the adsorption of As(III) was very fast from 15 to 150 min for all studied concentrations and achieved equilibrium at 150 min. Beyond equilibrium time of 150 min, the removal percentage became approximately constant due to unavailability of active sites. The removal percentage increased from 49.51 to 95.35%, 44.19 to 93.33%, 39.78 to 89.98%, 34.61 to 83.3% and 28.81 to 78.55% for initial As(III) concentration of 200, 400, 600, 800 and 1,000 μg/L, respectively. Because of the high availability of ample energetic sites on the AGSC surface, the rate of adsorption of As (III) ions was very sharp in the early stages.

2-2. Effect of Initial pH

In the adsorption process, the initial pH of the adsorbate solution plays a vital role in the removal percentage of target pollutant. In most of the cases, cations are best adsorbed at pH above the value of pH_{pzc} and anions are adsorbed at pH below pH_{pzc}. Due to the effect of pH in the adsorbate solution, both aqueous and surface chemistry of adsorbent are affected [33]. The removal of As(III) increased from 64.8 to 93.3% when the initial pH of the solution increased from 2.01 to 5.98. After that, it decreased with increasing the initial pH from 7.03 to 12.02. Similarly, the adsorption capacity of AGSC increased from 51.84 to 74.64 μg/g for increasing in initial pH from 2.01 to 5.98, and then adsorption capacity decreased as initial pH increased from 7.03 to 12.02, as shown in Fig. 5(b). Maximum adsorption occurred at pH of 5.98. The effect of initial pH on the removal of As(III) by AGSC can be described in two steps: (i) As(III) exists in solution as H_3AsO_3 at pH 0-9.2 while $H_2AsO_3^{1-}$, $HAsO_3^{2-}$ and AsO_3^{3-} ions exist as stable forms at pH 10-12, 13 and 14, respectively [34]. Therefore, As(III) adsorption is highly dependent on pH. The abundant available surface functional groups (-OH, -COOH, =CO, quinone and carboxylic anhydride) onto AGSC get protonated and form positively charged -OH_2^+, -$COOH_2^+$, =COH^+ after reaction with H^+ in acidic medium. Therefore, the acidic condition is not favorable for neutral H_3AsO_3 removal. In this situation, the removal percentage of As(III) ions was very low. On increasing the initial pH of the solution, the protonated groups on the AGSC surface decreased. For this reason the percentage removal of As(III) ions sharply increased till pH 6. (ii) After XPS analysis of the As3d spectra of arsenic loaded AGSC, it was found that As(V) was present in the sample. This result shows that the adsorption of As(III) on the AGSC is not only As(III) form, but it was also absorbed in the form of As(V). The reason for the presence of As(V) is due to the partial change in the oxidation state of As(III). As(V) is also found in the different state at different pH level, for example, $H_3AsO_4^o$, $H_2AsO_4^-$, $HAsO_4^{2-}$ and AsO_4^{3-} are found at pH 0-2, 2-7, 7-12 and 12-14, respectively. Due to the formation of $H_2AsO_4^-$ ions at pH range 2-7, the strong electrostatic force of attraction functioned between protonated surface functional groups and $H_2AsO_4^-$ ions. Therefore, the removal percentage of arsenic was increased on increasing the initial pH from 2 to 6. The adsorption capacity and removal percentage of arsenic onto AGSC were decreased when raising the initial pH of the solution from 6 to 12. This reduction may be due to the deproton-

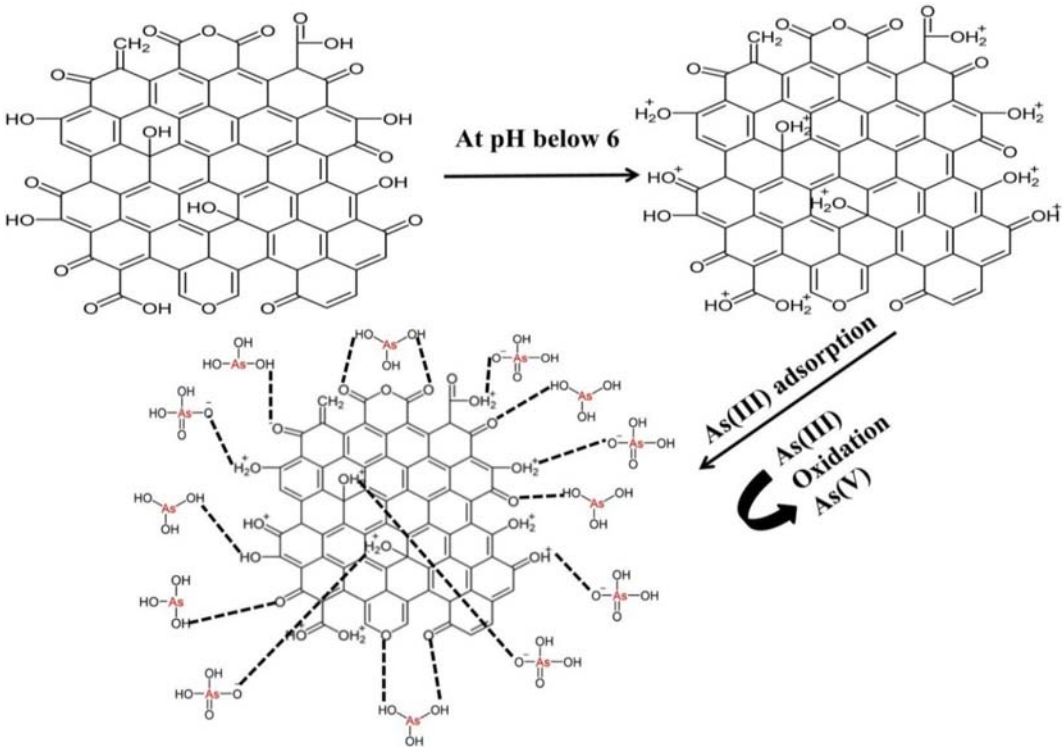

Fig. 4. Proposed reaction mechanism for As(III) adsorption onto AGSC adsorbent.

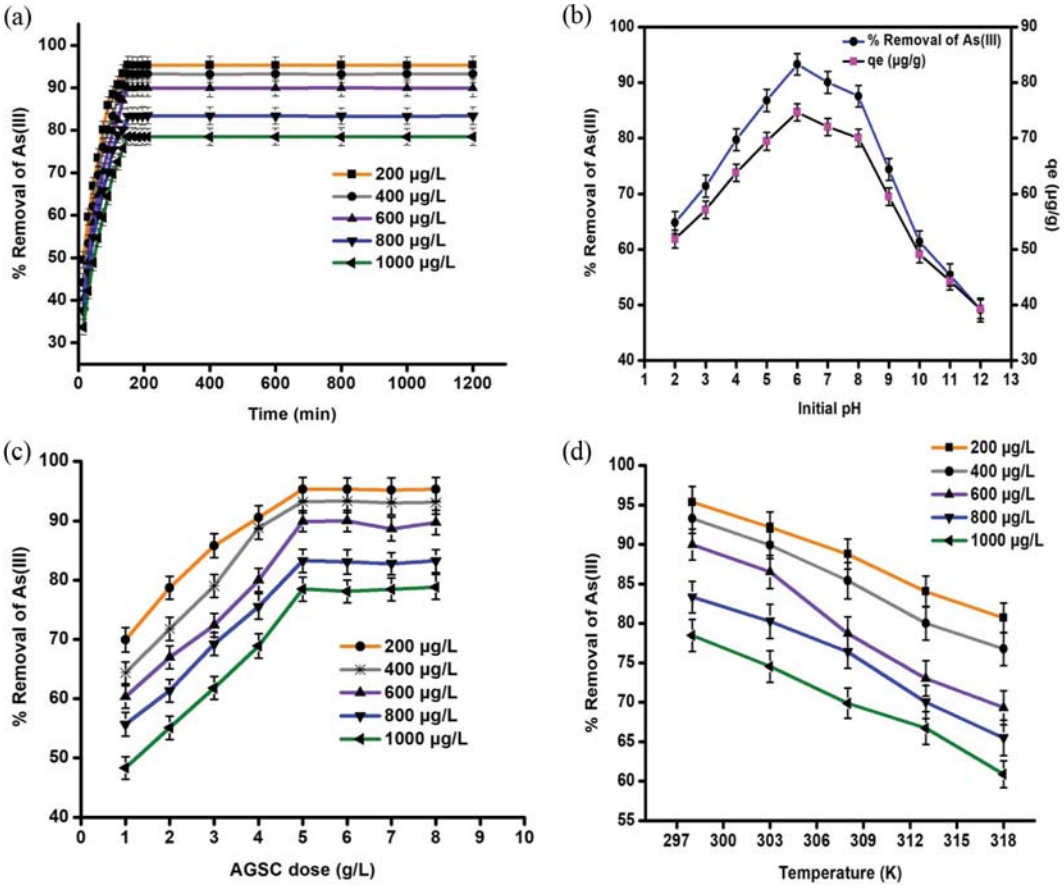

Fig. 5. Effect of (a) equilibrium time, (b) initial pH, (c) adsorbent dose and (d) temperature on adsorption of As(III) onto AGSC.

ation of functional groups on the ASGC in high pH. The pH_{pzc} for AGSC was 6.8, and this result indicated that the surface of AGSC possessed electro-positivity when the pH of the solution was less than 6.8 and electronegativity gradually increased on increasing initial pH of the solution from 6 to 12. Due to increasing electronegativity in solution, the repulsion force acting between the surface of AGSC and As(III)/As(V) ions was responsible for decreased adsorption capacity and arsenic removal at higher pH (alkaline) medium. The possible reaction mechanism for adsorption of arsenic species on AGSC is described in Fig. 4. A similar mechanism was suggested by Alam et al. [35], Chammui et al. [36].

2-3. Effect of Initial As(III) Concentration and Adsorbent Dose

Fig. 5(c) shows the effect of a change in the initial concentration of As(III) ions on the percentage removal of As(III) by AGSC. Adsorption phenomenon of As(III) ions mainly depends on active sites of functional groups and pores available on the surface of AGSC adsorbent because adsorption occurs on these sites and pores of the AGSC. A fixed quantity of AGSC dose has a constant number of active sites and on increasing adsorbate concentrations; the active sites become saturated, so increasing As(III) concentration does not increase the adsorption efficiency. Percentage removal was maximum for a particular concentration after which increase in the concentration of As(III) decreased the removal of As(III), as illustrated in Fig. 5(c). Due to low As(III) ion/adsorbent ratios, As(III) ion adsorption involved higher active sites. For increasing As(III) ions/adsorbent ratio, the higher active sites were saturated by As(III) ions, and adsorption began at lower energy sites. The initial rate of external diffusion decreased and the rate of intra-particle diffusion increased as the initial concentration of As(III) increased. A similar result was reported by Nemr et al. [37].

With increased AGSC adsorbent dose, the removal percentage of As(III) ions increased up to 5 g/L adsorbent dose. After that, there was no effective increase in the removal of As(III) ions on increasing adsorbent dose after 5 g/L. The percentage removal of As(III) ions was increased mainly due to the high availability of both active functional sites and surface area of the AGSC adsorbent with the increased dose of AGSC. Due to the availability of highly active functional binding sites, arsenic species would form a complexation [38]. The additional increment in AGSC dose did not cause a significant improvement in the removal percentage because there was a shortage of As(III) ions in the solution while the active site and surface area increased with AGSC dose [39]. Therefore, it showed a negligible dose effect on As(III) removal after 5 g/L AGSC adsorbent dose.

2-4. Effect of Temperature

The temperature has a substantial effect on the phenomenon of adsorption. Most of the adsorption process is exothermic and shows a decreasing trend in the removal percentage with the rise in temperature. The results presented in Fig. 5(d) confirm that the removal percentage of As(III) decreased with increase in temperature, and the maximum removal of 95.32% was found at 298 K for 200 μg/L initial As(III) concentration. The decrease in the removal percentage of As(III) ions with the rise in temperature was due to the increasing Brownian motion and breaks in intermolecular hydrogen bonding between arsenic and AGSC molecules in the adsorbate solution. For this reason, the removal percentage decreased in raising temperature [40].

3. Adsorption Kinetics Modeling and Isotherms

3-1. Kinetics Study for Adsorption of As(III) onto AGSC

The dynamics of adsorption process describes the rate of As(III) uptake by the AGSC, which controls the equilibrium time. Kinetic studies were done to understand the rate-determining step and transport mechanism such as mass transfer of molecules from liquid to solid phase during the batch adsorption process. In the present study, pseudo-first-order, pseudo-second-order and Elovich models were adopted to describe the adsorption of As(III) onto AGSC. Batch experiments were carried out at different time intervals (15-150 min) with changing initial As(III) concentration from 200 to 1,000 μg/L by keeping all the other parameters (such as initial pH, AGSC dose, speed of incubator and temperature of solution) constant.

3-2. Pseudo-first-order Model

Pseudo-first-order (Lagergren) model showed the kinetic rate

Table 1. Nonlinear and linear form of equation of kinetic and mass transfer models

	Equation in nonlinear form	Equation in linear form	Equation no.
Kinetic models			
Pseudo-first-order (Lagergren) model	$q_t = q_e(1-e^{-k_1 t})$	$\log(q_e - q_t) = \log q_e - \frac{k_1 t}{2.303}$	3
Pseudo-second-order model	$q_t = \frac{q_e^2 k_2 t}{q_e k_2 t + 1}$	$\frac{t}{q_t} = \frac{t}{q_e} + \frac{1}{k_2 q_e^2}$	4
Elovich kinetics	$q_t = \frac{1}{\beta}(\ln(\alpha\beta t))$	$q_t = \frac{1}{\beta}\ln(\alpha\beta) + \frac{1}{\beta}\ln t$	5
Mass transfer mechanism models			
Weber & Morris model		$q_t = k_{id} t^{0.5} + C$	6
Boyd model		$\ln(1-F) = -k_{fd} t$	7

q_e=experimental adsorption capacity (μg/g) at equilibrium; q_t=adsorption capacity (μg/g) at time t; k_1=rate constant for pseudo-first-order model (min^{-1}): k_2=rate constant for pseudo-second-order adsorption model (g/μg·min); α=initial desorption rate (μg/g·min); β=desorption constant (g/μg); k_{id}=intra-particle diffusion rate constant; C=intercept (μg/g); F=fraction of solute adsorbed at any time t ($F=q_t/q_e$, dimensionless); k_{fd}=liquid film diffusion constant (sec^{-1})

equation for the adsorption of the solute particle on the surface of adsorbent is based on the uptake or adsorption capacity of the adsorbent. Lagergren first-order rate equation is one of the most commonly used rates kinetic equation for adsorption of adsorbate from a liquid to the solid phase. According to this model, initially, As(III) ions are not existent on the surface of AGSC, and as the adsorption process starts, As(III) ions start accumulating on the surface of AGSC and the accumulation continues until the adsorption

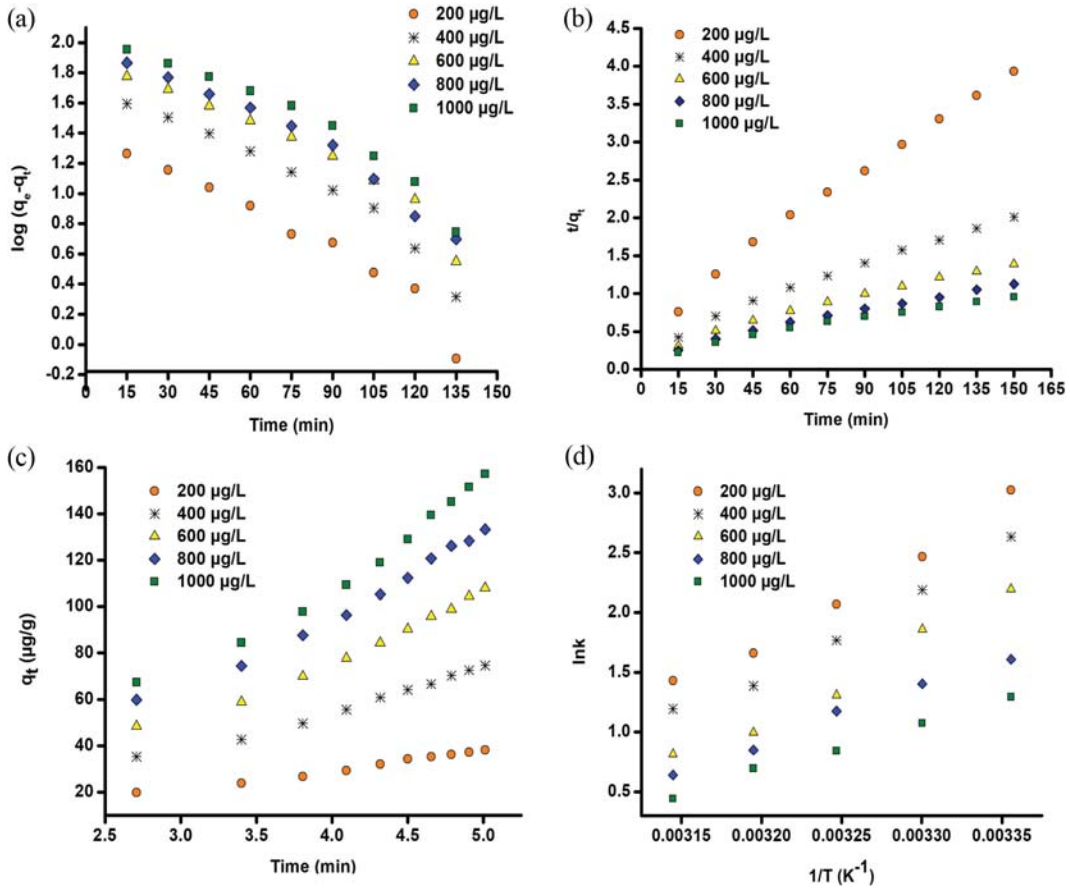

Fig. 6. Adsorption kinetic models (a) pseudo-first-order, (b) pseudo-second-order, (c) elovich and (d) van't Hoff plots for the adsorption of As(III) onto AGSC.

Table 2. Kinetic parameters of As(III) adsorption onto AGSC

Kinetic model	Parameters	Initial concentration (µg/L)				
		200	400	600	800	1000
Pseudo-first-order	$q_{e,exp}$ (µg/g)	38.144	74.64	107.988	133.33	156.96
	$q_{e,cal}$ (µg/g)	30.841	68.52	99.6093	125.19	155.23
	k_1	0.0235	0.0230	0.0212	0.0225	0.0216
	R^2	0.949	0.9536	0.943	0.9687	0.9463
	Standard error	0.07522	0.07011	0.0725	0.05613	0.0715
Pseudo-second-order	$q_{e,cal}$ (µg/g)	44.052	88.496	129.87	161.29	192.31
	k_2 (g/(µg·min))	$8.9*10^{-4}$	$3.6*10^{-4}$	$2.2*10^{-4}$	$1.8*10^{-4}$	$1.3*10^{-5}$
	V_o (µg/g·min)	1.73	2.8123	3.652	4.636	4.8614
	R^2	0.9948	0.992	0.9885	0.9903	0.984
	Standard error	0.0539	0.03347	0.02747	0.02035	0.02181
Elovich	β (g/µg)	0.119	0.0560	0.0374	0.0301	0.0248
	α (µg/g min)	5.133	7.320	8.995	11.31	11.573
	R^2	0.987	0.9847	0.9801	0.983	0.973
	Standard error	1.4600	3.3605	5.7511	6.6019	10.1665

process reaches equilibrium. The rate constant parameter and theoretical adsorption capacity of adsorption were calculated using Lagergren's kinetic equation [41]. Eq. (3) in Table 1 indicates the nonlinear and linear form of this model.

The value of k_1 and adsorption capacity q_e could be obtained from the slope and intercept of the plot between log ($q_e - q_t$) and time (t) as shown in Fig. 6(a). If the experimental adsorption capacity does not approximate to calculate adsorption capacity, then the adsorption process is not likely to be fit for the pseudo-first-order modal even higher value of correlation coefficient (R^2) [42]. Table 2 shows that the value of k_1 decreased as the initial concentration of As(III) increased. The k_1 values ranged from 0.0235 to 0.0216 min^{-1}. The experimental q_e values were much higher than theoretical q_e values shown in Table 2. Therefore, this model could be unfit for adsorption of As(III) ions onto AGSC.

3-3. Pseudo-second-order Model

The pseudo-second-order is also an important kinetic model which describes the adsorption dynamics of the process. This model assumes that chemisorption is the rate determining step and the q_e (uptake or adsorption capacity) is proportional to the number of the available active functional sites engaged on the surface of the adsorbent. According to the Azizian derivation, the adsorption process follows this model when the initial solution concentration of a solute is low [43,44]. The nonlinear and linear form of the pseudo-second-order model can be expressed by Eq. (4) in Table 1.

The straight-line plot of t/q_e against t (Fig. 6(b)) was used to determine the value of k_2 and q_e from the slope and intercept. It can be observed from the Table 2 that the values of correlation coefficient (R^2) for this model were higher than 0.98 at all initial As(III) concentrations, which indicates that the adsorption process of As(III) ions onto AGSC followed the pseudo-second-order model. Moreover, the calculated adsorption capacity values, 44.052, 88.496, 129.87, 161.29 and 192.31 μg/g at 200, 400, 600, 800 and 1,000 μg/L As(III) initial concentration, respectively, were close to the experimental adsorption capacity (Table 2). The adsorption affinity or initial rate constant ($V_o = k_2 q_e^2$) provides information about the adsorption rate at the beginning. It ranged from 1.73 to 4.8614 μg/g·min. The value of k_2 decreases with increasing $q_{e,cal}$ and V_o values when the concentration of As(III) increases from 200 to 1,000 μg/L. This result recommended that the adsorption of As(III) was faster at the initial period of time as the As(III) concentration was increased.

3-4. Elovich Kinetic Model

Elovich kinetic model is usually tested for chemisorption [45]. Nonlinear and linear forms of this model are given in Eq. (5) in Table 1. These constants were obtained from the slope and intercept of a linear plot between q_t vs. lnt (Fig. 6(c)). The R^2 values of Elovich kinetic are much lower than the R^2 values of the above two models (Table 2). Therefore, this model shows its unsuitability for the interpretation of experimental results.

3-5. Adsorption Isotherms of As(III) Removal by AGSC

The adsorption isotherm describes the most critical information, which includes the mechanism of adsorption and distribution policy of As(III) ions between solid and liquid phases at the point when the adsorption process achieves equilibrium [46]. The current research focused on understanding the adsorption nature

Table 3. Comparative evaluation of various adsorbents with AGSC for As(III) removal

Adsorbent	Surface area (m^2/g)	Optimum pH	Concentration of As(III) (mg/L)	Isotherm model	Adsorption capacity (mg/g)	Reference
Fly ash-based zeolite-reduced graphene oxide composite	-	8	0.01-0.03	Redlich-Peterson	0.049-0.146	48
Nano aluminum doped manganese copper ferrite Polymer	-	6	0.02-0.2	Freundlich model	0.053	49
Granular ferric hydroxide	112	7.6	0.005	Langmuir and Freundlich isotherms	0.112	50
Iron oxide coated sand	-	7.5	0.1-0.8	Langmuir isotherm	0.029	51
Calcium chloride impregnated rice husk carbon	101-173	10-11	0.1-1	Freundlich isotherm	0.0021-0.0183	22
Fe-hydrotalcite Supported magnetite Nanoparticle	38.5	9	0.1-2.0	Langmuir isotherm	0.121	52
Zinc loaded pine cone biochar	11.54	4	0.05-0.2	Langmuir isotherm	0.007	53
Pyrolyzed sewage sludge	70	3-3.5	0.1	Langmuir isotherm	0.07	54
Fe impregnated biochar (anaerobic granular sludge)	-	3.6	50	-	10.4	55
Fe-Mn modified biochar (FMBC)	208.6	7	0.2-50	Freundlich and Langmuir isotherms	8.25	56
AGSC	228	6	0.2-1.0	Langmuir and Temkin isotherms	0.192	Present study

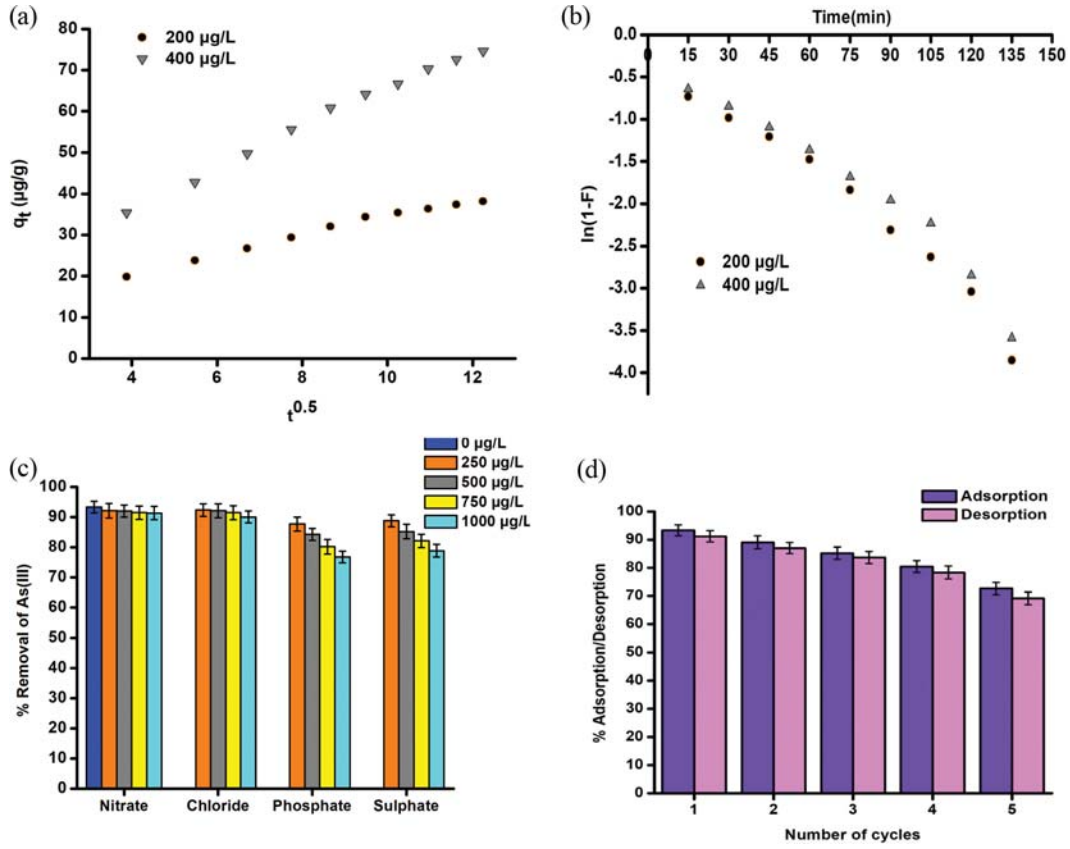

Fig. 7. (a) Weber & Morris model, (b) Boyd model, (c) effect of co-existing anions and (d) adsorption-desorption study of AGSC.

of AGSC adsorbent for As(III) removal. Langmuir, Temkin, and Freundlich isotherm models were investigated using experimental isotherm data (Table S5; detailed information of Langmuir, Temkin, and Freundlich isotherm models in Supporting Information). At 298 K temperature, for 400 µg/L of initial As(III) concentration (50 ml) and fixed AGSC dose (0.25 g) the experimental, Langmuir, Freundlich, and Temkin adsorption capacities (theoretical adsorption capacities) were found to be 74.64, 73.972, 67.6657 and 111.72 µg/L, respectively. So according to the correlation coefficient (R^2) from Table 6S and proximity of the theoretical to the experimental adsorption capacity, it can be concluded that the experimental data were best fitted to both Langmuir and Temkin models than to Freundlich isotherm. The aptness of both Langmuir and Temkin isotherm models indicates that AGSC adsorbent contains both homogeneous and heterogeneous active sites of functional groups because both models are based on surface homogeneity and heterogeneity, respectively. A similar result was also reported by Lam et al. regarding the removal of nickel ions by using the *Lansium domesticum* peel adsorbent [47]. The adsorption capacity of As(III) onto AGSC was compared with other adsorbents with their experimental conditions and physical properties as listed in Table 3.

4. Mass Transfer Mechanism and Thermodynamic Studies for As(III) Adsorption

The adsorption process is a part of the mass transfer operations. Hence, mass transfer is very important to explain its mechanism of As(III) ions transfer from the liquid phase to AGSC adsorbent solid phase. The shifting of the solute particle can be supported by either the intra-particle diffusion or film diffusion or sometimes by the combination of both [57]. Weber & Morris and Boyd models were used to determine the mass transfer mechanism of As(III) adsorption by AGSC adsorbent in this work.

4-1. Weber and Morris Model

Weber and Morris model is also known as the intra-particle diffusion model, as given by Eq. (6) in Table 1. A high C value suggests that the boundary layer has a more significant effect. The values of k_{id} and C can be calculated from the slope and intercept of the plot between q_t vs. $t^{0.5}$ (Fig. 7(a)). Application of this model confirms the dominance of intra-particle diffusion. If the plot of q_t vs. $t^{0.5}$ is linear and passing through the origin, then the mass transfer rate is controlled only by intra-particle diffusion. If the plot is linear or non-linear but does not pass through the origin, then two or more steps are used to control the mass transfer rate [58]. Table 4 shows the values of k_{id} and C. The R^2 values are 0.9937 and 0.9862 for the initial As(III) concentration of 200 and 400 µg/L, respectively, which are confirming that the Weber intra-particle diffusion controls the adsorption of As(III) on AGSC at low concentration. The value of rate constant of pore diffusion (k_{id}) and intercept (C) increased as the initial As(III) concentration increased from 200 to 400 µg/L (Table 4). This phenomenon happens due to the high value of boundary layer thickness and driving force associated with the initial As(III) concentration. The line did not pass

Table 4. Mass transfer parameter and correlation coefficients for removal of As(III) onto AGSC

	Mass transfer parameters					
	Weber & Morris model			Boyd model		
Co (μg/L)	k_{id} (μg/g·min$^{1/2}$)	R^2	C_1 (intercept)	k_{fd} (sec^{-1})	R^2	C_2 (intercept)
200	2.2472	0.9862	11.781	0.0248	0.9687	−0.1452
400	4.7917	0.9937	17.538	0.0229	0.9536	−0.0867

Table 5. Estimated values of ΔG^o, ΔH^o and ΔS^o for adsorption of As(III) onto AGSC

Parameter				Temperature (K)				
C_o (μg/L)	ΔH^o (kJ/mol)	ΔS^o (J/mol·K)	R^2	ΔG^o (kJ/mol)				
				298±2	303±2	308±2	313±2	318±2
200	−63.044	−187.0899	0.9854	−7.489	−6.218	−5.294	−4.320	−3.784
400	−58.119	−173.546	0.9868	−6.525	−5.512	−4.527	−3.609	−3.157
600	−57.269	−174.11	0.9762	−5.441	−4.685	−3.351	−2.590	−2.155
800	−39.226	−117.984	0.9919	−3.986	−3.535	−3.009	−2.208	−1.693
1000	−32.775	−99.24	0.9950	−3.205	−2.704	−2.156	−1.811	−1.170

through the origin, thus indicating the possibility of film diffusion along with inter-particle diffusion for As(III) adsorption.

4-2. Boyd Model

The Boyd diffusion model was employed to categorize film and inter-particle diffusion. Boyd diffusion model understands the mechanism of film diffusion during adsorption [59]. The linearized equation is expressed by Eq. (7) in Table 1. From the linear plot slope between ln(1−F) and t (Fig. 7(b)), the k_{fd} value can be calculated. For the initial As(III) concentration of 200 and 400 μg/L, the R^2 values are 0.9687 and 0.9536, respectively (Table 4). The line representing Boyd model did not pass through the origin, confirming that the adsorption of As(III) onto AGSC is not only controlled by the film diffusion.

4-3. Thermodynamic Studies

The analysis of the thermodynamic parameters could provide information concerning the nature of energy and structural change during the adsorption of As(III) ions onto AGSC [60]. The standard Gibbs free energy change (ΔG^0) is the major thermodynamic parameter for determining whether the adsorption process will occur or not. A negative value of ΔG^0 shows spontaneity and feasibility of chemical reaction at an appropriate temperature. The following equations estimated the thermodynamic properties such as a change in standard Gibbs free energy change (ΔG^0), change in standard entropy (ΔS^0) and change in standard enthalpy (ΔH^0) for As(III) adsorption [61]:

$$\Delta G^0 = \Delta H^0 - T\Delta S^0 \tag{8}$$

$$\Delta G^0 = -RT\ln K_0 \tag{9}$$

$$\ln K_0 = -\frac{\Delta H^0}{RT} + \frac{\Delta S^0}{R} \tag{10}$$

where, T, R and K_0 (dimensionless) are temperatures in Kelvin (K) scale, universal gas constant (8.314 J/mol·K) and thermodynamic equilibrium constant, respectively. The K_o value can be calculated from Eq. (11):

$$K_o = \frac{C_{ad,\,eq}}{C_{eq}} \tag{11}$$

where $C_{ad,\,eq}$ (μg/L) and C_{eq} (μg/L) are the equilibrium concentration of As(III) ions after adsorption of As(III) onto AGSC and equilibrium concentration of As(III) ions in solution, respectively. The experiments were performed at 298, 303, 308, 313 and 318 K, and it was observed from data that the K_o value decreased on increasing the temperature. The values of ΔS^0 and ΔH^0 were calculated from linear plots of ln K_0 vs. 1/T known as the van't Hoff plots, which are presented in Fig. 6(d) [62]. Table 5 shows all values of thermodynamic parameters. The high negative values of ΔG^0 at all evaluated temperatures indicate that the As(III) adsorption on AGSC is spontaneous. The less negative values of ΔG^0 on increasing temperature from 298 to 318 K means that adsorption of As(III) onto AGSC is spontaneous but less feasible at higher temperatures. Similarly, at different initial concentrations of As(III) (200 to 1,000 μg/L), the ΔG^0 values were negative (−1.170 to −7.489 kJ/mol) indicating that the process was spontaneous for all initial As(III) concentrations. The lowest value of ΔG^0 was obtained at 200 g/L and 298 K, which showed a high removal potential for As(III). The negative value of ΔH^0 (−63.04 to −32.78) indicates the exothermic nature of adsorption as also evident from the decrease of adsorption of As(III) with increasing temperature. A negative value of ΔS^0 (−187.09 to −99.24 J/mol·K) reveals decreased randomness at the solid-liquid interface during the adsorption of As(III) onto AGSC.

5. Effect of Co-existing Anions and Regeneration Studies

5-1. Effect of Co-existing Anions

In the groundwater, many ionic species are present along with the target pollutant. Thus, these ionic species may hinder the adsorption capacity of AGSC for arsenic via the emulative accumulation or binding with AGSC adsorbent, which affected the result of arsenic removal by AGSC adsorbent [63]. Batch experiments were performed to understand the individual separate effect of co-exist-

Table 6. Analysis of real groundwater sample of ghazipur district

Before treatment									
Sample collected	pH	Na^+ (mg/L)	K^+ (mg/L)	Ca^+ (mg/L)	SO_4^- (mg/L)	Cl^- (mg/L)	NO_3^- (mg/L)	Fe (mg/L)	As (μg/L)
Rajapur	7.52	41.4±2	10±1.5	61.2±1.8	74.4±4.8	178.8±4.2	2.45±0.21	0.41±0.06	137.5±5.2
Gahmar	7.60	50.1±25	13±2.1	72.7±2.8	106.5±3.2	92.6±3.5	7.9±0.45	0.79±0.04	67.3±4.6
After adsorption of the above sample using AGSC adsorbent under optimum condition									
Rajapur	7.21	32.4±1.2	8±0.5	51.8±1.3	36.2±2.4	134.4±3.1	2.01±0.12	0.29±0.08	8.5±1.4
Gahmar	7.24	43.7±2.1	10±1.7	60.5±2.0	74.3±2.9	62±2.7	6.5±0.31	0.61±0.11	6.7±1.1

ing anions such as sulfate, phosphate, chloride and nitrate on adsorption of As(III) by AGSC adsorbent. The impact of competing anions was studied at low to high (250 to 1,000 μg/L) concentration of these anions under the optimum condition of the experiment (Fig. 7(c)). The chemicals used in the present study included NaCl, Na_2SO_4, Na_2HPO_4 and $NaNO_3$ as the source of these anions. The removal percentage of As(III) was compared with the absence of co-existing ions (blank) to the samples having the presence of co-existing ions (Fig. 7(c)). It was observed from Fig. 7(c) that the presence of NO_3^- ions had no considerable effect on As(III) adsorption onto AGSC adsorbent in the concentration range of 250-1,000 μg/L. This is because the As(III) binding affinity for AGSC adsorbent is much higher than nitrate [64]. In the presence of chloride anions, no substantial effect shows on As(III) removal by AGSC. It happened because of the competing monovalent anion of chloride did not clash with As(III) ions. Sulfate, a divalent oxyanion, has a rivalry with arsenic ions due to electrostatic attraction force with AGSC. Therefore, sulfate has a profound impact on adsorption of As(III) onto AGSC adsorbent. Approximately 5-15% reduction in removal percentage was seen when the sulfate concentration was 250-1,000 μg/L in solution [65]. The presence of phosphate also profoundly influenced the removal percentage of As(III) ions, and many researchers also reported similar results [66-68]. The decrease in removal percentage was found to be 6-18% when the range of phosphate concentration increased from 250 to 1,000 μg/L. This is due to high charge density and comparable size of phosphate and arsenite oxyanions. The phosphate provides competition for identical active sites of AGSC adsorbent [21]. However, phosphate ions are absent or rarely occur in the groundwater, so its impact on As(III) removal should not be an issue [69].

5-2. Desorption and Regeneration Studies of AGSC Adsorbent

The reuse of adsorbent is necessary for the feasibility and economical operation of the water treatment system. That is why the study of desorption was carried out with As(III) loaded AGSC at different concentrations of NaOH solution. On increasing the pH of the solution, the increased number of OH^- ions resulted in more release of As(III) ions in the solution. Hence, 0.05 to 2.5 M NaOH solution was used to desorb the adsorbed As(III) from AGSC. From Fig. 4S, 60.87% of adsorbed As(III) was found to be desorbed at 0.05 M NaOH solution. On the increase in NaOH concentration up to 1 M, 91.21% of As(III) was released from AGSC and then decreased on increasing the concentration of NaOH. Reusability studies of regenerated adsorbent were also done and it was found that approximately 73% of Arsenic was removed in the fifth cycle (Fig. 7(d)). Due to the high adsorption-desorption rate, AGSC is an excellent adsorbent for the removal of arsenic.

6. Analysis and Treatment of Real Groundwater Sample

AGSC adsorption efficiency was also investigated for the removal of arsenic from real groundwater samples. Real groundwater samples were collected from two blocks: Rajapur and Gahmar from Ghazipur district, Uttar Pradesh, India. Ghazipur district is highly influenced by arsenic pollution in groundwater. The concentration of arsenic and other chemicals present in these two groundwater samples are listed in Table 6. The results of the AGSC treated sample are also listed in Table 6.

CONCLUSION

AGSC was an effective adsorbent in treating As(III) contaminated synthetic water and as groundwater sample. It removed more than 94% of As(III) from groundwater under the optimum condition, which is below the permissible limit according to the guidelines of WHO. The greater surface area, high porosity, and the presence of various functional groups onto AGSC are responsible for the adsorption of As(III). In the FTIR spectrum of AGSC after adsorption, the peaks intensity and position were reduced and shifted, respectively; this illustrates that the adsorption of As(III) onto AGSC occurred. BET analysis revealed that most of the pores were found in the mesopores region in nano shape. These results were also confirmed by SEM analysis. The fitted XPS spectra of As3d showed that adsorption of arsenic onto AGSC occurred in the form of AS(III) and As(V). The effect of pH played an essential role in the removal percentage of arsenic ions from the water; removal percentage was the maximum on pH 6, and when the electronegativity of the solution increased, the percentage of removal decreases. The adsorption efficiency of AGSC for removal of arsenic (III) from the water was increased when enhanced adsorbent dose and equilibrium time up to 6 g/L and 150 min, respectively, and then it remained constant. Both Langmuir and Temkin models were best fitted with experimental data of adsorption process as compared to the Freundlich isotherm model. The pseudo-second-order kinetic described best As(III) adsorption onto AGSC as compared to pseudo-first-order and Elovich kinetic model. Thus, chemisorption phenomena might be the rate-limiting step for As(III) adsorption process. The mass transfer mechanism for As(III) adsorption onto AGSC showed the possibility of film diffusion along with interparticle diffusion. The thermodynamic study revealed the adsorption of As(III) on AGSC is exothermic and spontaneous. The As(III) adsorption was highly affected by the existence of

phosphate and sulfate. The regeneration of AGSC exhibited excellent desorption of 91.21% of As(III) at 1 M NaOH solution. Thus, AGSC is an effective adsorbent for removing low concentration range of As(III) ions from synthetic water.

ACKNOWLEDGEMENTS

Authors are grateful to Indian Institute of Technology (BHU), Varanasi, India, for providing the necessary facilities related to research work. The authors also express gratitude for the financial assistance provided by MHRD, India.

SUPPORTING INFORMATION

Additional information as noted in the text. This information is available via the Internet at http://www.springer.com/chemistry/journal/11814.

REFERENCES

1. S. Ayoob, A. K. Gupta and V. T. Bhat, *Crit. Rev. Environ. Sci. Technol.*, **38**, 401 (2008).
2. Y. Wang and D. C. W. Tsang, *J. Environ. Sci.*, **25**, 2291 (2013).
3. S. M. Cohen, L. L. Arnold, B. D. Beck, A. S. Lewis and M. Eldan, *Crit. Rev. Toxicol.*, **43**, 711 (2013).
4. World Health Organization (WHO)/UNICE, *Progress on drinking-water and sanitation* (2014).
5. M. Vithanage, I. Herath, S. Joseph, J. Bundschuh, N. Bolan, Y. S. Ok, M. B. Kirkham and J. Rinklebe, *Carbon*, **113**, 219 (2017).
6. P. L. Smedley and D. G. Kinniburgh, *Appl. Geochem.*, **17**, 517 (2002).
7. A. Kumar, J. Pandey and S. Kumar, *Korean J. Chem. Eng.*, **35**(2), 456 (2018).
8. T. Nawaz, M. Iqbal, S. Zulfiqar and M. I. Sarwar, *Korean J. Chem. Eng.*, **35**(6), 860 (2018).
9. N. N. Greenwood and A. Earnshaw, *Chemistry of the elements*, *3th Ed.*, Pergamon Press, Oxford, United Kingdom (1984).
10. World Health Organization (WHO), *Guidelines for Drinking-water Quality, 4th Ed.* (2011).
11. P. B. Tchounwou, B. Wilson and A. Ishaque, *Rev. Environ. Health*, **14**, 211 (1999).
12. J. E. Greenleaf, J. C. Lin and A. K. Sengupta, *Environ. Prog.*, **25**, 300 (2006).
13. J. W. Wang, D. Bejan and N. J. Bunce, *Environ. Sci. Technol.*, **37**, 4500 (2003).
14. V. Pallier, G. Feuillade-Cathalifaud, B. Serpaud and J. C. Bollinger, *J. Colloid Interface Sci.*, **342**, 26 (2011).
15. W. Wan, T. J. Pepping, T. Banerji, S. Chaudhari and D. E. Giammar, *Water Res.*, **45**, 384 (2011).
16. H. Park and H. Choi, *Water Res.*, **45**, 1933 (2011).
17. S. O. Lesmana, N. Febriana, F. E. Soetaredjo, J. Sunarso and S. Ismadji, *Biochem. Eng. J.*, **44**, 19 (2009).
18. M. Taheran, M. Naghdi, S. K. Brar, E. J. Knystautas, M. Verma, A. A. Ramirez, R. Y. Surampalli and J. R. Valero, *Sci. Total Environ.*, **571**, 772 (2016).
19. S. Liu, C. Ni, H. Su, H. Liu, R. Chen, P. Li and Y. Wei, *RSC Adv.*, **6**, 30840 (2016).
20. M. Thommes, K. Kaneko, A. V. Neimark, J. P. Olivier, F. Rodriguez-Reinoso, J. Rouquerol and K. S. W. Sing, *Pure Appl. Chem.*, **87**, 1051 (2015).
21. L. Li, X. L. Liu, H. Y. Geng, B. Hu, G. W. Song and Z. S. Xu, *J. Mater. Chem. A*, **1**, 10292 (2013).
22. P. Mondal, C. B. Majumder and B. Mohanty, *Ind. Eng. Chem. Res.*, **46**, 2550 (2007).
23. B. H. Hameed and A. A. Ahmad, *J. Hazard. Mater.*, **164**, 870 (2009).
24. J. Xua, L. Chena, H. Qu, Y. Jiao, J. Xie and G. Xing, *Appl. Surf. Sci.*, **320**, 674 (2014).
25. M. S. Podder and C. B. Majumdar, *J. Mol. Liq.*, **2**, 382 (2015).
26. C. Saka, *J. Anal. Appl. Pyrolysis*, **95**, 21 (2012).
27. A. Swiatkowski, M. Pakula, S. Biniak and M. Walczyk, *Carbon*, **42**, 3057 (2004).
28. Y. Su, X. Sun, X. Zhou, C. Dai and Y. Zhang, *J. Environ. Sci.*, **36**, 1 (2015).
29. H. Trevino-Cordero, L. G. Juarez-Aguilar, D. I. Mendoza-Castillo, V. Hernandez-Montoya, A. Bonilla-Petriciolet and M. A. Montes-Moran, *Ind. Crops Prod.*, **42**, 315 (2013).
30. S. Biniak, G. Szymanski, J. Siedlewski and A. Swiatkowski, *Carbon*, **35**, 1799 (1997).
31. J. H. Zhou, Z. J. Sui, J. Zhu, P. Li, D. Chen, Y. C. Dai and W. K. Yuan, *Carbon*, **45**, 785 (2007).
32. U. Shafique, A. Ijaz, M. Salman, W. Zaman, N. Jamil and R. Rehman, *J. Taiwan Inst. Chem. Eng.*, **43**, 256 (2012).
33. Z. Gu, J. Fang and B. Deng, *Environ. Sci. Technol.*, **39**, 3833 (2005).
34. J. Youngran, F. Maohong, J. V. Leeuwen and J. F. Belczyk, *J. Environ. Sci.*, **19**, 910 (2007).
35. M. A. Alam, W. A. Shaikh, M. O. Alam, T. Bhattacharya, S. Chakraborty, B. Show and I. Saha, *Appl. Water Sci.*, **8**, 198 (2018).
36. Y. Chammui, P. Sooksamiti, W. Naksata, S. Thiansem and O. Arqueropanyo, *Chem. Eng. J.*, **240**, 202 (2014).
37. A. E. Nemr, A. Khaled, O. Abdelwahab and A. El-Sikaily, *J. Hazard. Mater.*, **152**, 263 (2008).
38. M. D. Meitei and M. N. V. Prasad, *Ecol. Eng.*, **71**, 308 (2014).
39. A. Goswami, P. K. Raul and M. K. Purkait, *Chem. Eng. Res. Des.*, **90**, 1287 (2012).
40. H. Li, G. Huang, C. An, J. Hu and S. Yang, *Ind. Eng. Chem. Res.*, **52**, 15923 (2013).
41. M. K. Mondal, G. Mishra and P. Kumar, *J. Sustain. Dev. Energy Water Environ. Syst.*, **3**, 405 (2015).
42. V. Vadivelan and K. V. Kumar, *J. Colloid Interface Sci.*, **286**, 90 (2005).
43. S. Azizian, *J. Colloid Interface Sci.*, **276**, 47 (2004).
44. S. Srivastava, S. B. Agrawal and M. K. Mondal, *Korean J. Chem. Eng.*, **33**, 567 (2016).
45. C. Aharoni and F. C. Tompkins, *Adv. Catal.*, **21**, 1 (1970).
46. R. Narayan, R. P. Meena, A. K. Patel, A. K. Prajapati, S. Srivastava and M. K. Mondal, *Environ. Prog. Sustain. Energy*, **35**, 95 (2015).
47. Y. F. Lam, L. Y. Lee, S. J. Chua, C. S. Shee and S. Gan, *Ecotoxicol. Environ. Saf.*, **127**, 61 (2016).
48. R. Soni and D. P. Shukla, *Chemosphere*, **219**, 504 (2019).
49. M. A. Malana, R. B. Qureshi and M. N. Ashiq, *Chem. Eng. J.*, **172**, 721 (2011).
50. O. S. Thirunavukkarasu, T. Viraraghavan and K. S. Subramanian, *Water SA*, **29**, 161(2003).

51. V. K. Gupta, V. K. Saini and N. Jain, *J. Colloid Interface Sci.*, **288**, 55 (2005).
52. T. Turk and I. Alp, *J. Ind. Eng. Chem.*, **20**, 732 (2014).
53. N. V. Vinh, M. Zafar, S. K. Behera and H. S. Park, *Int. J. Environ. Sci. Technol.*, **12**, 1283 (2015).
54. D. S. Tavares, C. B. Lopes, J. P. Coelho, M. E. Sánchez, A. I. Garcia, A. C. Duarte, M. Otero and E. Pereira, *Water Air Soil Pollut.*, **223**, 2311 (2012).
55. M. E. Lee, P. Jeon, J. Kim and K. Baek, *Korean J. Chem. Eng.*, **35**(7), 1409 (2018).
56. L. Lin, W. Qiu, D. Wang, Q. Huang, Z. Song and H. W. Chau, *Ecotox. Environ. Safe.*, **144**, 514 (2017).
57. U. Maheshwari, B. Mathesan and S. Gupta, *Process Saf. Environ. Prot.*, **98**, 198 (2015).
58. W. J. Weber and J. C. Morris, *J. Sanit. Eng. Div.*, **89**, 31 (1993).
59. A. B. Albadarina, C. Mangwandi, A. A. H. Al-Muhtaseb, G. M. Walker, S. J. Allena and M. N. M. Ahmad, *Chem. Eng. J.*, **179**, 193 (2012).
60. S. Srivastava, S. B. Agrawal and M. K. Mondal, *Ecol. Eng.*, **85**, 56 (2015).
61. R. Foroutan, R. Mohammadi and B. Ramavandi, *Korean J. Chem. Eng.*, **35**(1), 234 (2018).
62. T. Keleti, *Biochem. J.*, **209**, 277 (1983).
63. P. B. Bhaskar, A. K. Gupta, S. Ayoob and S. Kandu, *Colloids Surf. A: Physicochemical. Eng. Aspects*, **281**, 237 (2006).
64. X. Yu, S. Tong, M. Ge, J. Zuo, C. Cao and W. Song, *J. Mater. Chem. A*, **1**, 959 (2013).
65. G. Zhang, J. Qu, H. Liu and R. Wu, *Water Res.*, **41**, 1921 (2007).
66. R. Prabhakar and S. R. Samadder, *J. Mol. Liq.*, **250**, 192 (2018).
67. S. Zhang, H. Niu, Y. Cai, X. Zhao and Y. Shi, *Chem. Eng. J.*, **158**, 599 (2010).
68. S. R. Chowdhury and E. K. Yanful, *J. Environ. Manage.*, **91**, 2238 (2010).
69. T. G. Asere, K. Verbeken, D. A. Tessema, F. Fufa, C. V. Stevens and G. D. Laing, *Environ. Sci. Pollut. Res.*, **24**, 20446 (2017).

Supporting Information

Hazardous As(III) removal using nanoporous activated carbon of waste garlic stem as adsorbent: Kinetic and mass transfer mechanisms

Anuj Kumar Prajapati and Monoj Kumar Mondal†

Department of Chemical Engineering and Technology, Indian Institute of Technology (Banaras Hindu University), Varanasi, Uttar Pradesh 221005, India
(*Received 9 April 2019 • accepted 28 August 2019*)

1. Adsorption Isotherms of As(III) Removal by AGSC

1-1. Langmuir Isotherm Model

The essential fundamental assumption of this model is that adsorption happens at energetically non- heterogeneous surfaces of adsorbent and forms a monolayer of adsorbate ions or particles on the adsorbent surface with the finite number of identical adsorption sites. Due to this assumption, the uptake of As(III) arises on homogeneous sites by monolayer adsorption and no interaction exists between the adsorbed ions [1]. Therefore, no further adsorption process can take place after the formation of adsorbate monolayer on the adsorbent surface [2]. Eq. (1) in Table S4 represents the nonlinear and linear form of the Langmuir isotherm equations. The Langmuir isotherm model characteristics index can be described by an equilibrium parameter or separation factor (R_L) which is a constant and dimensionless number represented by the Eq. (2) in Table S4 [3]. The value of separation factor (R_L) should lie in between 0 and 1 for the proper adsorption phenomenon [4].

The maximum adsorption capacity (q_m) and Langmuir constant K_L can be calculated from the plot between C_e/q_e and C_e, as shown in Fig. S1 and the calculated value of Langmuir parameters are presented in Table S5. The maximum Langmuir adsorption capacities (q_m (μg/g)) were calculated as 181.50, 185.18, 185.20,

Table S1. Experimental condition for As(III) adsorption onto AGSC

S. No.	Parameters used	Range of operating parameters				
		pH	AGSC dose (g/L)	Temperature (K)	Initial As(III) concentration (μg/L)	Equilibrium time (min)
1	Equilibrium time	6	5	298	200-1000	15-1200
2	Initial pH	2-12	5	298	400	150
3	AGSC dose	6	1-8	298	200-1000	150
4	Temperature	6	5	298-318	200-1000	150
5	Initial As(III) concentration	6	1-8	298	200-1000	150
6	Desorption	-	5	298	400	120

Table S2. BET analysis results of AGSC

Sample	S_{BET} (m^2/g)	S_{micro} (m^2/g)	S_{meso} (m^2/g)	V_{total} (cm^3/g)	V_{micro} (cm^3/g)	V_{mesol} (cm^3/g)	V_{micro}/V_{total} (%)	V_{meso}/V_{total} (%)	D_p (nm)
AGSC	227.62	203.00	28.58	0.12	0.10	0.02	86.19	13.81	2.09

Table S3. FTIR spectrum peaks before and after adsorption of As (III) onto AGSC

Frequency (cm^{-1})			Functional groups
Before adsorption	After adsorption	Differences	
3449.8	3439.5	10.3	O-H stretching (phenols, alcohols)
2923.7	2924.9	1.2	C-H stretching (aliphatic or aldehyde carbon)
2360.4	2362.8	2.8	C≡C stretching (alkyne groups)
1634.3	1627.1	7.2	N-H out of plane bend (amide groups)
1388.8	1384.4	4.4	-CH_3 stretching (alkanes)
873.5	884.5	11	-C-H out of plane (aromatic ring)

Table S4. Binding energy (BE) and relative content (%) of C1s, O1s and As3d according to the XPS fitted spectrum of AGSC

Peak intensity	XPS binding energy (eV)	Possible chemical groups/element with oxidation state	Relative area (%)
		Fitted C1s and O1s XPS spectra of AGSC before As(III) adsorption	
C 1s (90.78)*	284.6	C=C (sp^2 hybridized)	84.13
	286.7	C-OH (carbon present in alcohol or ether groups)	5.76
	287.5	C=O (carbon in carboxyl or ester groups)	4.79
	289.3	-COOH, C=O (carbon in carbonyl or quinone groups)	5.32
O 1s (9.22)*	531.1	C=O (carbonyl oxygen of quinone)	22.05
	532.2	C-OH (carbonyl oxygen in ester, anhydride, and hydroxyl groups)	28.35
	533.3	C-O-C (Non-carbonyl oxygen atom in esters and anhydrides)	29.97
	534.4	COOH (oxygen atom in carboxyl groups)	18.23
	536.2	adsorbed water/oxygen	1.40
		Fitted As3d XPS spectra of AGSC after As(III) adsorption	
As 3d	44.6	As (III)	55.74
	45.8	As (V)	44.26

*Atomic percentage (AP) of carbon, oxygen from XPS data

192.30 and 172.41 corresponding to the temperature 298, 303, 308, 313 and 318 K, respectively. The values of K_L were found as 0.0256, 0.0157, 0.0097, 0.0060 and 0.0057 L/μg at 298, 303, 308, 313 and 318 K, respectively. These low values of K_L indicated good binding capacity of As(III) ions onto the surface of AGSC at different temperatures. It is clear from Table S5 that the Langmuir isotherm model was exhibiting highest correlation coefficient (R^2) values at all experimental temperatures indicating best fitted to the experimental data. In the present study, the separation factor (R_L) was ranged from 0.03 to 0.46, which elicited favorable condition for adsorption at all temperatures. However, on increasing the temperature, R_L value was also increased, and the lowest R_L value was obtained at 298 K, suggesting that the process of absorption at high temperatures was less favorable.

1-2. Freundlich Isotherm Model

The Freundlich isotherm [5] can be utilized for non-ideal adsorption that includes heterogeneous surface energy system. Unlike Langmuir isotherm, it is based on multilayer adsorption. It gives the exponential distribution of active sites and suggesting that enthalpy of adsorption is independent of the mass of pollutant species adsorbed. Freundlich model states that the equilibrium capacity of adsorbent (q_e) is directly proportional to $1/n^{th}$ power of equilibrium concentration (C_e) as given by the Eq. (3) in Table S4 (non-linear and linear).

The values of Freundlich constants K_f, n and linear regression correlation (R^2) were determined from the plot of $\ln q_e$ vs. $\ln C_e$ as shown in Fig. S2. These constants of the model cannot explain the chemo-Phys properties of the adsorption phenomenon [6]. Table S5 shows the values of these constants and K_f values of As(III) ions decreased as the temperature increased, which showed that the process of adsorption was favored at low temperature.

The magnitude of n lies between 2.27and 1.77 therefore the value of 1/n lies between 0 and 1 indicating that the adsorption of As(III) ions onto AGSC is favorable. When the value of 1/n reaches to 0

Table S5. Nonlinear and linear form of equation of isotherm models

	Equation in nonlinear form	Equation in linear form	Equation No.
Isotherm models			
Langmuir isotherm	$q_e = \frac{q_m K_L C_e}{1 + K_L C_e}$	$\frac{C_e}{q_e} = \frac{C_e}{q_m} + \frac{1}{q_m K_L}$	1
		$R_L = \frac{1}{1 + K_L C_O}$	2
Freundlich isotherm	$q_e = K_f C_e^{1/n}$	$\ln q_e = \ln K_f + \frac{1}{n} \ln C_e$	3
Tempkin isotherm	$q_e = B * \ln(AC_e)$	$q_e = B \ln A + B \ln C_e$	4
		$B\left(= \frac{RT}{b}\right)$	

q_e=experimental adsorption capacity (μg/g) at equilibrium; q_m=maximum adsorption capacity (g/g) of AGSC (theoretical adsorption capacity); K_L is an Langmuir constant (L/g); C_e=equilibrium As(III) concentration (μg/L) in the liquid phase; C_o=initial As(III) concentration; K_f= Freundlich model constants; 1/n=heterogeneity factor constant; R=universal gas constant; T=temperature (K); A=equilibrium binding constant (L/μg); B=Tempkin constant related to the enthalpy of adsorption; b=Tempkin isotherm constant

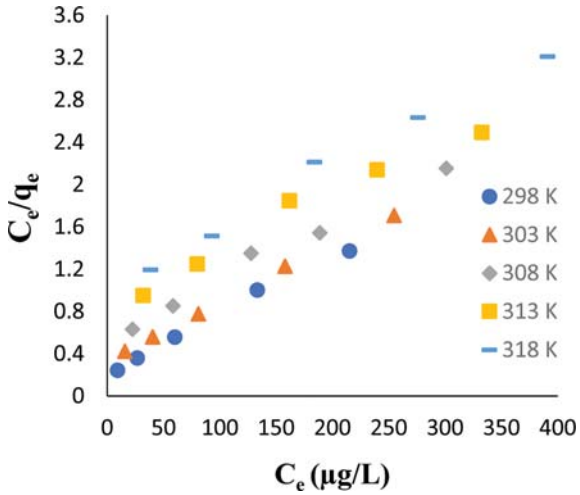

Fig. S1. Langmuir isotherm for the adsorption of As(III) onto AGSC.

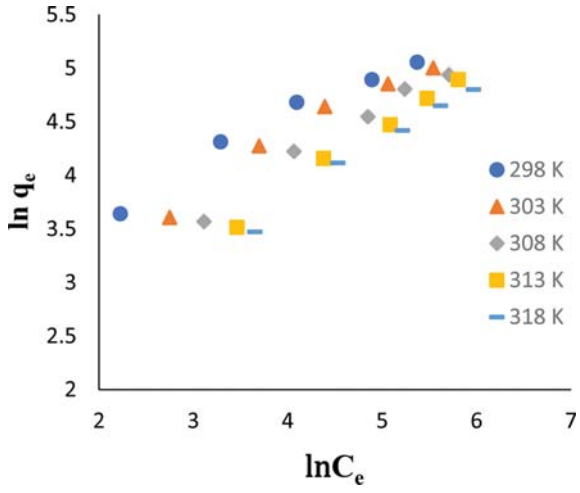

Fig. S2. Freundlich isotherm for the adsorption of As(III) onto AGSC.

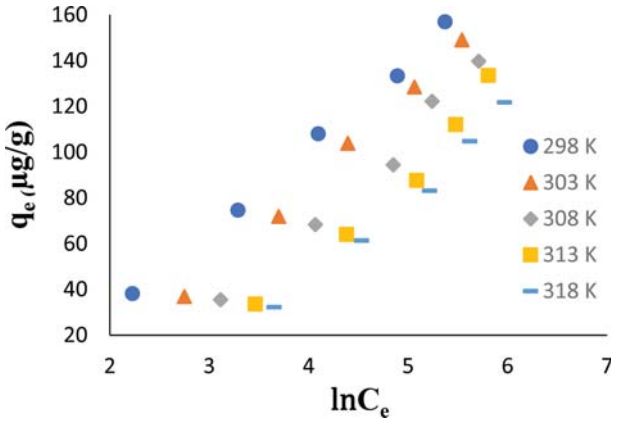

Fig. S3. Tempkin isotherm for the adsorption of As(III) onto AGSC.

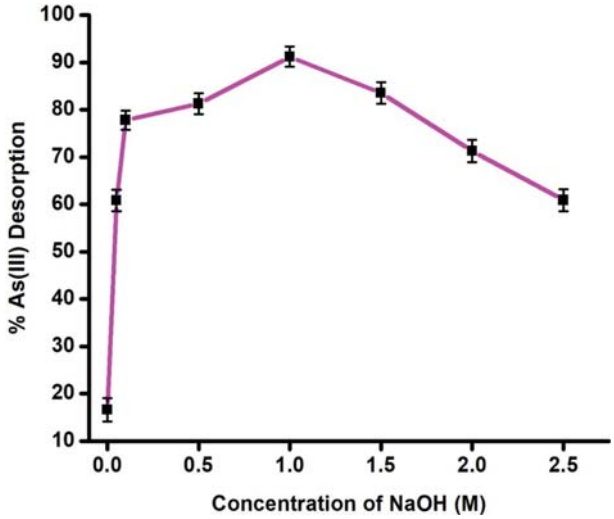

Fig. S4. Desorption study of As(III) loaded AGSC.

Table S6. Isotherm model constants and correlation coefficient for adsorption of As(III) onto AGSC

Isotherm model	Parameters	Temperature (K)				
		298±2	303±2	308±2	313±2	318±2
Langmuir isotherm	q_m (µg/g)	181.80	185.18	185.20	192.30	172.41
	K_L (L/µg)	0.0256	0.0157	0.0097	0.0060	0.0057
	R_L	0.16-0.03	0.24-0.06	0.34-0.09	0.45-0.14	0.46-0.15
	R^2	0.995	0.999	0.989	0.980	0.990
	Standard error	0.0252	0.01416	0.05502	0.0935	0.0542
Freundlich isotherm	K_f[(µg/g)/(µg/L)$^{1/n}$]	15.9061	10.498	7.2623	4.718	4.3146
	n	2.27117	2.0169	1.887	1.7301	1.7652
	R^2	0.968	0.968	0.985	0.993	0.989
	Standard error	0.1896	0.2339	0.1776	0.1327	0.15674
Tempkin isotherm	B	37.366	40.354	40.4	41.356	39.674
	A (L/µg)	0.2894	0.1559	0.0987	0.0633	0.0532
	R^2	0.997	0.998	0.985	0.974	0.976
	Standard error	4.5976	3.5256	13.4135	19.1731	12.3746

that means the adsorbent surface is more heterogeneous and when the values of n lie between 1<n<10 it confirms the physical and favorable nature of adsorption [7]. The Freundlich isotherm model did not fit well with the experimental results because of low correlation coefficients (R^2) at all evaluated temperatures.

1-3. Tempkin and Pyzhev Isotherm Model

According to Tempkin and Pyzhev isotherm, due to adsorbent-adsorbate interactions, particle adsorption heat on the layer decreases linearly with coverage. The binding energies are homogeneously distributed [8]. The Tempkin and Pyzhev isotherm model for both non-linear and linear forms are represented by the Eq. (4) in Table S5.

The values of Tempkin constant A and B were calculated from the plots between q_e vs. $\ln C_e$, as shown in Fig. 3S. The results obtained from the plots are represented in Table 5S. The high value of correlation coefficient (R^2) indicated that the Tempkin model was well fitted with experimental data at different temperatures. The values of Tempkin constant A (L/μg) was found to decrease with increase in temperature, which indicated lower binding energy at an elevated temperature that confirmed adsorption of As(III) onto AGSC was suitable at low temperature.

REFERENCES

1. K. K. Singh, R. Rastogi and S. H. Hasan, *J. Hazard. Mater.*, **121**, 51 (2005).
2. I. Langmuir, *J. Am. Chem. Soc.*, **38**, 2221 (1916).
3. S. V. Ramanaiah, S. V. Mohan and P. N. Sarma, *Ecol. Eng.*, **31**, 47 (2007).
4. S. Lunge, S. Singh and A. Sinha, *J. Magn. Magn. Mater.*, **356**, 21 (2014).
5. H. M. F. Freundlich, *J. Phys. Chem.*, **57**, 385 (1906).
6. S. Kundu and A. K. Gupta, *Chem. Eng. J.*, **122**, 93 (2006).
7. F. Nekouei, S. Nekouei, I. Tyagi and V. K. Gupta, *J. Mol. Liq.*, **201**, 124 (2015).
8. F. Cloak, N. Atar and A. Olgun, *Chem. Eng. J.*, **150**, 122 (2009).